Sonochemical Approach to the Synthesis of Fe_3O_4@SiO_2 Core–Shell Nanoparticles with Tunable Properties

Anne-Laure Morel,[†] Sergei I. Nikitenko,[†,*] Karine Gionnet,[‡] Alain Wattiaux,[§] Josephine Lai-Kee-Him,[⊥] Christine Labrugere,[§] Bernard Chevalier,[§] Gerard Deleris,[†] Cyril Petibois,[†] Alain Brisson,[⊥] and Monique Simonoff[†]

[†]CNAB, UMR 5084, Université Bordeaux I, II, CNRS, Le Haut Vigneau, 33170 Gradignan, France, [‡]LMMA, INSERM, U920, Université Bordeaux I, Bât. B2, Av. des Facultés, 33405 Talence cedex, France, [§]ICMCB, Université Bordeaux I, CNRS, 87, avenue du Dr. A. Schweitzer, 33608 Pessac cedex, France, and [⊥]CBHN, UMR 5248, Université Bordeaux I, ENITAB, IECB, Bât. B8, Av. des Facultés, 33402 Talence cedex, France

ABSTRACT In this study, we report a rapid sonochemical synthesis of monodisperse nonaggregated Fe_3O_4@SiO_2 magnetic nanoparticles (NPs). We found that coprecipitation of Fe(II) and Fe(III) in aqueous solutions under the effect of power ultrasound yields smaller Fe_3O_4 NPs with a narrow size distribution (4–8 nm) compared to the silent reaction. Moreover, the coating of Fe_3O_4 NPs with silica using an alkaline hydrolysis of tetraethyl orthosilicate in ethanol–water mixture is accelerated many-fold in the presence of a 20 kHz ultrasonic field. The thickness of the silica shell can be easily controlled in the range of several nanometers during sonication. Mössbauer spectra revealed that nonsuperparamagnetic behavior of obtained core–shell NPs is mostly related to the dipole–dipole interactions of magnetic cores and not to the particle size effect. Core–shell Fe_3O_4@SiO_2 NPs prepared with sonochemistry exhibit a higher magnetization value than that for NPs obtained under silent conditions owing to better control of the deposited silica quantities as well as to the high speed of sonochemical coating, which prevents the magnetite from oxidizing.

KEYWORDS: magnetite · silica · core–shell nanoparticles · sonochemistry · ultrasound · Mössbauer spectroscopy · FT-IR · XPS

Magnetic iron oxide nanoparticles (NPs) have attracted much research interest over the recent years because of their unique physicochemical properties and great potential for various biomedical applications. In several pioneering works magnetic NPs were claimed as an effective tool for magnetically assisted biomolecule separation,[1] biochemical sensing,[2] NMR imaging,[3,4] targeted drug delivery,[5,6] and magnetic hyperthermia.[7,8] Furthermore, a novel application of magnetic NPs for tissue engineering, termed "magnetic force-based tissue engineering (Mag-TE)" has been proposed recently.[9]

The requirements for any biomedical application of magnetic colloids include the chemical stability, biocompatibility, strong magnetization, and low coercivity of the dispersed magnetic NPs. In principal, silica-coated magnetite NPs, Fe_3O_4@SiO_2, comply with these requirements. The outer shell of silica not only protects the inner magnetite core from oxidation but also provides sites for surface functionalization with poly(ethylene glycol) and various biomolecules. For *in vivo* applications magnetic core–shell NPs should have a limiting size in the order of 20–50 nm to be able to migrate across the reticuloendothelial system and to be stealthy toward the mononuclear phagocyte system.[3,7]

There are essentially two methods for the coating of Fe_3O_4 NPs with silica: by acidic hydrolysis of silicate in aqueous solutions and by a modified Stöber process[10] which consists of the alkaline hydrolysis of tetraethyl orthosilicate (TEOS) in ethanol/water mixture in the presence of Fe_3O_4 NPs. Deposition of silica from silicate solution usually yields relatively big spherical magnetic particles with a mean size in the range of 80–200 nm.[11–13] These particles are useful for biomolecule separation or sensing *in vitro* but cannot be delivered intravenously. In the seminal work of Philipse and coworkers[14] it was shown that Fe_3O_4@SiO_2 NPs with the mean diameter of 60–120 nm can be obtained by the Stöber process from initial 5–15 nm size Fe_3O_4 precursors only after the bare magnetite particles were pretreated with a small amount of silicate in an aqueous solution. Without this procedure, coating with TEOS in ethanol– aqueous ammonia mixture yields magnetite clusters embedded in large silica aggregates. The thin silica layer at the Fe_3O_4 NPs surface reduces the isoelectric point of magnetite and thus maintains the colloidal stability during the second coating. However, the silicate precoating is not a sufficient condition to obtain the uniform

*Address correspondence to nikitenk@cenbg.in2p3.fr.

Received for review February 13, 2008 and accepted April 09, 2008.

Published online May 27, 2008.
10.1021/nn800091q CCC: $40.75

core−shell NPs. It was shown[14] that the concentration of pretreated magnetite particles should be less than 12 mg · L^{-1}, otherwise large aggregates of magnetite are formed in TEOS solutions. The Fe_3O_4@SiO_2 NPs prepared by the Stöber process usually contain about six Fe_3O_4 cores even under optimal conditions.[14] Further detailed studies of Fe_3O_4 NPs coating using TEOS[15−17] revealed the high sensitivity of this process to experimental conditions such as ethanol/water ratio, concentration of ammonia and TEOS, and temperature, *etc.* Moreover, the coating of Fe_3O_4 NPs with silica using TEOS was found to be a very slow process: from 12 to 48 h of mechanical stirring at room temperature is necessary to obtain uniform a silica shell on the surface of magnetite NPs. Heating of the reacting mixture causes formation of big magnetite−silica aggregates with irregular morphology. To improve the homogeneity of silica-coated iron oxide NPs and to increase the limiting concentration of NPs in reaction medium several authors used a modified Stöber process in reverse microemulsion conditions.[18,19] However, this method also requires at least 20−24 h of aging to obtain the final product and much effort to separate core−shell NPs from the large amount of surfactants associated with the microemulsion system.

In this work, we report the use of sonochemistry for the rapid synthesis of monodispersed Fe_3O_4@SiO_2 NPs with tunable properties using the Stöber process. The term sonochemistry is used to describe chemical processes occurring in liquids under the effect of power ultrasound. For the ultrasonic frequencies usually employed to influence chemical processes (20−60 kHz), the wavelengths produced in the liquid medium are in the range of 7.5 to 3.0 cm or considerably longer than the chemical bond length values. Therefore, the chemical effects of ultrasound are not the result of direct interactions between the molecules and the sonic waves. The origin of sonochemistry derives from acoustic cavitation, that is, formation, growth, and implosive collapse of gas-filled microbubbles in a liquid subjected to ultrasonic irradiation.[20,21] Transient collapse generates high peak temperatures (~5000 K) within the cavitation bubbles and overheating of the interfacial region around the bubbles (~200 nm) until several hundred degrees, as well as the intense shock waves emanated upon collapse. Since the collapse occurs in less than a microsecond, very high cooling rates, in excess of 10^{10} K, are obtained. For these reasons, treatment of solutions with power ultrasound not only offers the possibility to disperse friable solids in the liquids but also provides a unique set of conditions to produce unusual materials from dissolved volatile and nonvolatile precursors. After the pioneering work of Suslick and co-workers on amorphous iron preparation by $Fe(CO)_5$ sonolysis[22] a large number of nanosized metals, metal alloys, oxides, carbides, and sulfides were prepared using sonochemical reactions with volatile metal−carbonyls in appropriate organic solvents.[20,23] On the other hand, sonochemistry was proven to be effective for NPs insertion into mesoporous matrixes and NPs deposition on ceramic and polymeric supports.[20,23] Magnetite NPs were prepared by sonolysis of $Fe(CO)_5$ in aqueous medium in the presence of sodium dodecyl sulfate[24] and by sonochemical oxidation of Fe(II) in aqueous solutions.[25,26] Very recently it was shown that ultrasonic treatment enhances the uniformity of SiO_2 NPs obtained by TEOS hydrolysis[27] and improves the coating of SiO_2 microspheres with FePt alloy[28] and FeNi fine particles with silica.[29]

This paper reports that the sonochemical approach provides a resolution of several important problems in the synthesis of Fe_3O_4@SiO_2 NPs by the Stöber process related to the necessity of silicate pretreatment, the slow kinetics, and the risk of aggregates formation. Moreover, the thickness of the silica shell over Fe_3O_4 NPs can be easily tuned during sonication which is important in order to avoid magnetite nanoparticles oxidation and agglomeration. It is known that the superparamagnetism of uncoated single domain magnetic particles can vanish because of the intergrain magnetic dipole interaction.[30] In the absence of an external magnetic field the energy of dipole−dipole monodomain attraction is given by[31]

$$V(r) = -V^2_{max}(r)/6kt \quad (1)$$

where $V^2_{max}(r)$ is a maximal attraction energy in a head-to-tail configuration and r is a distance between the centers of two monodomains. If a magnetic core is coated by an insulating shell the dipole−dipole attractions become negligible for some critical diameter of a insulating sphere σ_B (Boyle diameter):[14]

$$\sigma^3_B = \alpha d^6/(6kt)^{1/2} \quad (2)$$

where d is a magnetic core diameter, $\alpha = M^2\pi/72\mu_0$, M is a volume saturation magnetization, and μ_0 is the permeability of a vacuum. From eq 2 it follows, for example, that for $d = 10$ nm the dispersion of Fe_3O_4@SiO_2 NPs should be stable and superparamagnetic if $\sigma \geq 25$ nm. Here, we present the evidence that the superparamagnetic behavior of Fe_3O_4@SiO_2 NPs can be tailored by the silica shell thickness.

RESULTS AND DISCUSSION

Preparation of Fe_3O_4 NPs. The bare Fe_3O_4 NPs were prepared by the well-known Massart's method[32] which consists of Fe(III) and Fe(II) coprecipitation in alkaline solutions:

$$2Fe(III) + Fe(II) + 8OH^- \rightarrow Fe_3O_4 + 8H_2O \quad (3)$$

The only difference in our method was the application of ultrasonic irradiation at 20 kHz instead of mechanical

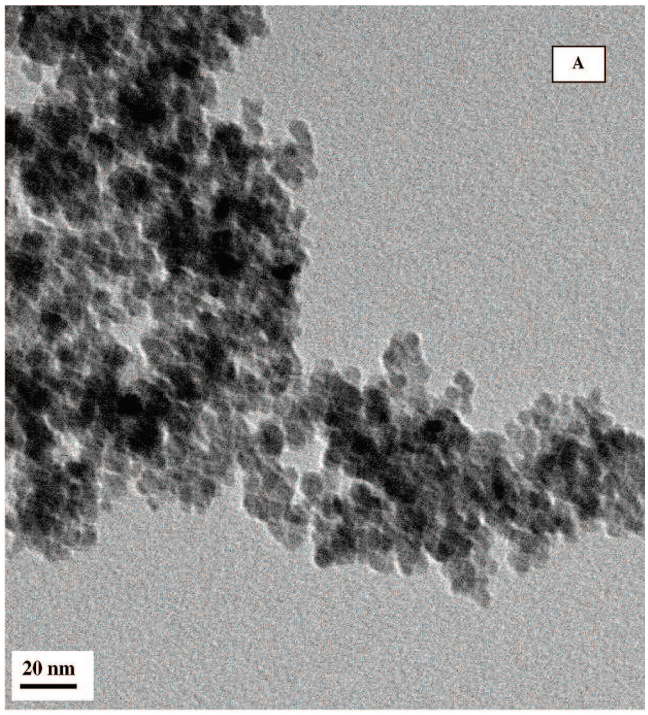

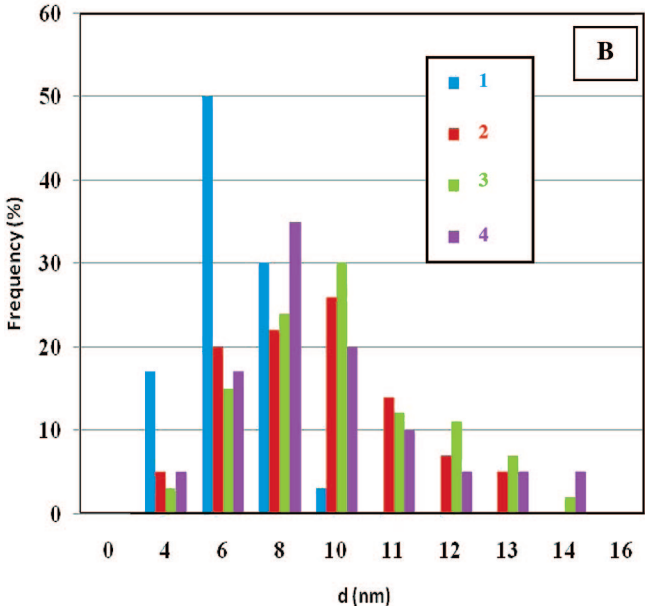

Figure 1. (a) TEM image of Fe_3O_4 NPs obtained by ultrasonically assisted coprecipitation. An Fe(II)/Fe(III) mixture was injected into the active cavitation zone. Scale bar = 20 nm. (b) The size histograms of Fe_3O_4 NPs obtained under ultrasound ($[Fe_3O_4] = 1.7 \times 10^{-2}$ M, $[NH_3 \cdot H_2O] = 2$ M, $[N_2H_4 \cdot H_2O] = 0.01$ M, $T = 30-32$ °C, $f = 20$ kHz, $I = 30$ W·cm^{-2}, $P_{ac} = 0.67$ W·mL^{-1}) by Fe(II)/Fe(III) mixture injection into the active cavitation zone (1) or in the upper part of the sonoreactor outside of the active cavitation zone (2) and mechanical stirring ($[Fe_3O_4] = 5 \times 10^{-3}$ M, $[NH_3 \cdot H_2O] = 1$ M, room temperature, ref 14 (3); $[Fe_3O_4] = 4 \times 10^{-2}$ M, $[NH_3 \cdot H_2O] = 1$ M, room temperature, ref 33 (4).

agitation during the synthesis. Figure 1 demonstrates the transmission electron microscopy (TEM) image and the size histograms for Fe_3O_4 NPs prepared with and without ultrasound at similar conditions. It can be seen that precipitation under power ultrasound yields particles that are smaller and have more narrow size distribution as compared to those prepared by mechanical stirring. Particle size histograms reveal that the effect of ultrasound on the magnetite particles size is observed much more clearly if the mixture of Fe(II) and Fe(III) is injected directly into the active cavitation zone of the sonoreactor. A TEM image of polymodal Fe_3O_4 NPs obtained with ultrasound but when the Fe(II)/Fe(III) mixture was injected outside of the active cavitation zone is presented in the Supporting Information. The particle size histogram for this case is very similar to that obtained under mechanical stirring.

The active zone of the sonoreactor is shown in Figure 2. A clearly visible cloudlike region with the maximal concentration of cavitation bubbles has a circular cone shape which is "stuck" to the radiating surface of the titanium horn. Obviously, the maximal effect of ultrasound should be observed in this "cone-bubble structure".[21] Moreover, Fe(II)/Fe(III) coprecipitation is known to be a quasi-immediate process.[33,34] Therefore, to observe the effect of ultrasound on magnetite precipitation and the hydrolysis of iron ions and magnetite particles, nucleation should occur in the active zone of acoustic cavitation to avoid interference with coprecipitation in the bulk solution in the absence of cavitation. Recently it was assumed that three effects of sonication contribute to the phenomenon of sonocrystallization:[35,36] (i) the local transient heating of a liquid after bubble collapse, (ii) the shock waves generated during bubbles implosion hinder agglomeration, and (iii) the excellent mixing conditions created by acoustic cavitation. All these phenomena allow a reduction of particle size and increase particle size homogeneity owing to control of the local nucleus population.

The Fe2p high resolution XPS spectrum of Fe_3O_4 NPs precipitated under ultrasound (Figure 3) reveals that, in contrast to γ-Fe_2O_3 (Aldrich) XPS spectrum, it does not contain the charge transfer satellite of $Fe2p_{3/2}$ at 720 eV indicating formation of a mixed oxide of Fe(II) and Fe(III), such as Fe_3O_4.[37] That confirms the relatively low extent of Fe_3O_4 NPs surface oxidation during precipitation under ultrasound. The binding energy (E_B) for $Fe2p_{3/2}$ photoelectrons (711.2 eV) of the synthesized NPs is very close to that published in the literature (710.6 eV).[37]

Sonochemical Coating of Fe_3O_4 NPs with Silica. Sonication of Fe_3O_4 NPs suspension in alkaline ethanol−water solutions of TEOS causes rapid coating of the magnetic

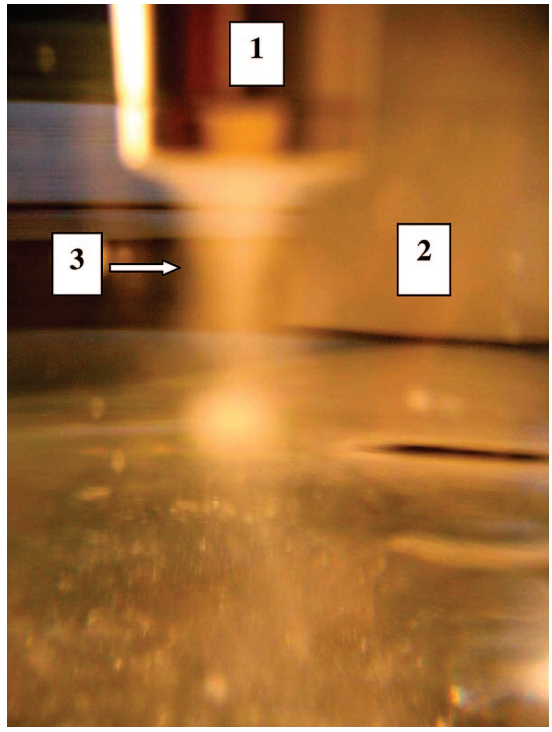

Figure 2. Image of the active cavitation zone of the sonoreactor (f = 20 kHz, I = 30 W · cm^{-2}, P_{ac} = 0.67 W · mL^{-1}). (1) Titanium ultrasonic horn, (2) sonicated water in the thermostatted cell under argon, (3) "cone bubble structure" of the active cavitation zone.

core with a silica shell. FT-IR spectra of the solid products demonstrate the increase of absorbance at 1080 cm^{-1} attributed to ν_{as}(Si−O−Si) vibrations[38] during sonication. The calibration curve for FT-IR quantitative silica analyses is shown in Supporting Information. Figure 4 reveals that the concentration of deposited silica increases linearly with the time of sonochemical treatment indicating zero-order kinetics of SiO_2 formation.

Moreover, sonication causes at least 5-fold acceleration of TEOS hydrolysis compared to the silent reaction at similar experimental conditions.

The XPS spectra of Fe $2p_{3/2}$ ($E_B \approx 711$ eV) and Si 2p ($E_B \approx 103$ eV) core−electrons gives a further proof for the rapid Fe_3O_4 NPs coating with silica under ultrasound. Data in Table 1 clearly show the increase of Si 2p peak intensity during sonication. At the same time the peak intensity of Fe $2p_{3/2}$ sharply decreases until its practical disappearance during 3 h of sonication. The XPS surveys of Fe_3O_4@SiO_2 NPs are shown in Supporting Information.

TEM images of Fe_3O_4@SiO_2 NPs (Figure 5) demonstrate the increase of silica shell thickness with sonication time in a good agreement with FT-IR and XPS measurements. According to TEM measurements the silica shell thickness is increased from 1.0−1.5 nm after 1 h of sonication to 3.0−3.5 nm after 3 h of ultrasonic treatment. Also TEM images reveal that the magnetic cores are not collapsed under sonication. Silica particles without magnetic cores are not observed indicating the heterogeneous mechanism of silica nucleation and growth at the magnetite surface. It is worth noting that practically all core−shell particles obtained with ultrasound contain a single magnetic core. By contrast, the TEM image presented in Supporting Information indicates that TEOS hydrolysis in the presence of Fe_3O_4 NPs under mechanical stirring and without silicate pretreatment causes formation of big irregular aggregates with the extremely heterogeneous distribution of silica in full agreement with published data.[14] It should be emphasized that the overheating of the reaction mixture yields big aggregates even under ultrasound. The TEM image presented in the Supporting Information shows the typical cluster of Fe_3O_4 NPs embedded in silica ob-

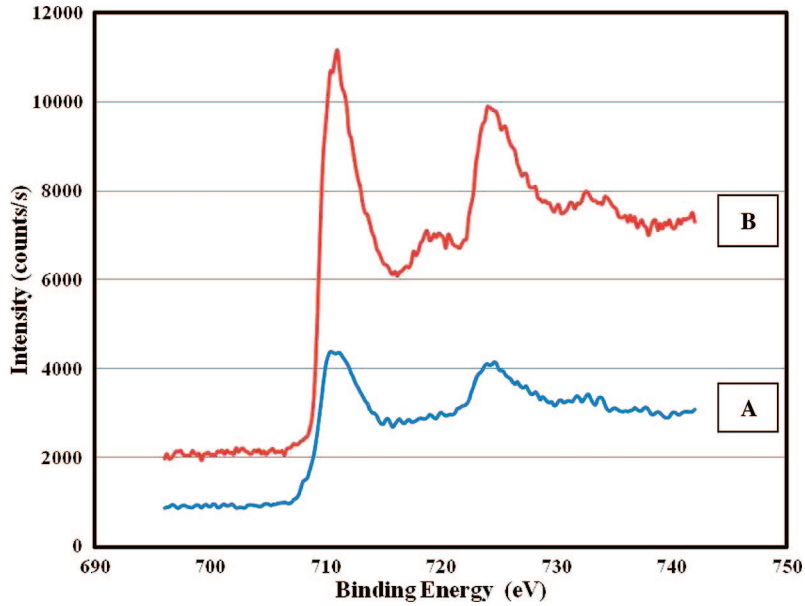

Figure 3. Fe 2p high resolution XPS spectra for (A) Fe_3O_4 NPs obtained under ultrasound and (B) γ-Fe_2O_3 provided by Aldrich.

TABLE 1. Surface Concentration of Fe and Si for Fe_3O_4@SiO_2 NPs Obtained by XPS Technique

	atomic %	
particles	Si2p	Fe $2p_{3/2}$
Fe_3O_4	0	15.3
Fe_3O_4@SiO_2, 1 h of ultrasound	13.3	11.8
Fe_3O_4@SiO_2, 3 h of ultrasound	26.5	0.6

TABLE 2. Hydrodynamic Diameter of Fe_3O_4@SiO_2 NPs as a Function of the Sonication Time Measured Using Dynamic Light Scattering in EtOH

particles	hydrodynamic diameter (nm)	polydispersity index (r.u.)
Fe_3O_4@SiO_2, 1 h of ultrasound	49	0.01
Fe_3O_4@SiO_2, 3 h of ultrasound	53	0.12

tained after 2 h of sonication at 45 °C. It appears that the increase of temperature of the bulk solution causes acceleration of the undesirable homogeneous silica nucleation followed by the aggregation of Fe_3O_4@SiO_2 and SiO_2 NPs.

The values of hydrodynamic diameter for Fe_3O_4@SiO_2 NPs measured with dynamic light scattering (DLS) in ethanol are summarized in Table 2. Particle size distribution curves exhibit only one peak with a small polydispersity index indicating the low extent of Fe_3O_4@SiO_2 NPs aggregation in solutions. The hydrodynamic diameter of the particles is approximately three times larger than that measured with TEM. This difference may be due to the particles solvation and dynamic association in the liquid. Roughly, such associates contain on average three single Fe_3O_4@SiO_2 NPs. The slight increase of hydrodynamic diameter with the time of sonication is correlated with the increase of silica shell thickness.

Probable Mechanism of TEOS Sonochemical Hydrolysis. The significant acceleration of TEOS alkaline hydrolysis under the effect of power ultrasound could be understood in light of the two-site model of the sonochemical reactions:[39] the dominant site is the cavitation bubble interior gas-phase while the secondary site is a liquid shell surrounding the cavitation bubble. The resonance size of a bubble in the solvents with low viscosity, like water, alkanes, or ethanol, sonicated at 20 kHz is approximately 150−200 μm[21] and the liquid reaction zone extends approximately 200 nm (500 molecules)[39] from the bubble surface. The lifetime of the overheated liquid zone is less than 2 μs after collapse. When the acoustic pressure from the ultrasonic waves decreases, the gas bubble is expanded, and gas or vapors flow into the bubble from the liquid in its neighborhood. At our experimental conditions the cavitation bubbles are filled with argon, ethanol, water, ammonia, and TEOS vapors. The vapor pressure

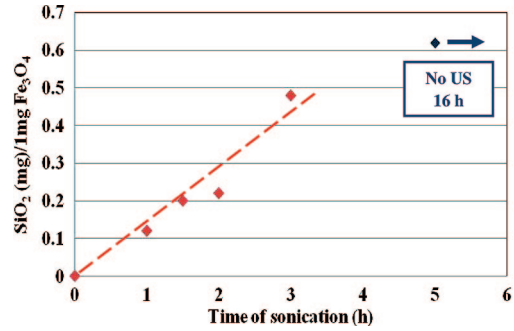

Figure 4. Kinetics of SiO_2 sonochemical deposition on Fe_3O_4 NPs in EtOH/$NH_3 \cdot H_2O$ solutions. [Fe_3O_4] = 7.8 × 10^{-3} M, [TEOS] = 4.0 × 10^{-2} M, [$NH_3 \cdot H_2O$] = 0.225 M, [H_2O] = 12.35 M, f = 20 kHz, I = 30 W · cm^{-2}, P_{ac} = 0.67 W · mL^{-1}, T = 32 °C, Ar. The blue diamond corresponds to the SiO_2 concentration deposited under silent conditions at intensive mechanical nonmagnetic stirring during 16 h under similar conditions.

of ethanol (bp 78 °C) at 32 °C is much higher than that of TEOS (bp 158 °C). Consequently, the concentration of TEOS molecules within the bubble is negligibly low and the sonochemically driven hydrolysis of TEOS, most probably, occurs in the liquid reaction zone and not in the gas-phase of the cavitation bubble. The Stöber process can be cast as hydrolysis eq 4 and condensation polymerization eq 5 steps:

$$Si(OR)_4 + 4H_2O \rightarrow Si(OH)_4 + 4ROH \quad (4)$$

$$nSi(OH)_4 \rightarrow n(SiO_2) + 2nH_2O \quad (5)$$

In the presence of catalysts, hydrolysis of TEOS is generally faster than the condensation reaction. However, usually they cannot be separated. The overall TEOS hydrolysis in ethanol−water mixture is known to be temperature sensitive:[27] heating to 70 °C causes a significant increase in the reaction rate. As a consequence, transient temperature jumps in the liquid shell surrounding the cavitation bubble would lead to strong local acceleration of silica nucleation.

Furthermore, ultrasonically forced oscillations of the cavitation bubble can push ultrasmall particles to the bubble surface during the expansion half-cycle by a process similar to rectified diffusion described above for gases and vapors. This suggests that the liquid reaction zone surrounding the cavitation bubble is enriched with Fe_3O_4 NPs which play a role of scavenger for silica nucleus. The presumable mechanism of sonochemical coating is shown schematically in Figure 6. Otherwise cold bulk solution avoids the secondary irregular nucleation of silica. Moreover, the significant acceleration of mass transport created by acoustic cavitation improves the homogeneity and monodispersity of core−shell particles.

Tailoring the Magnetic Properties of Fe_3O_4@SiO_2 NPs. Mössbauer spectra of bare Fe_3O_4 NPs at room temperature

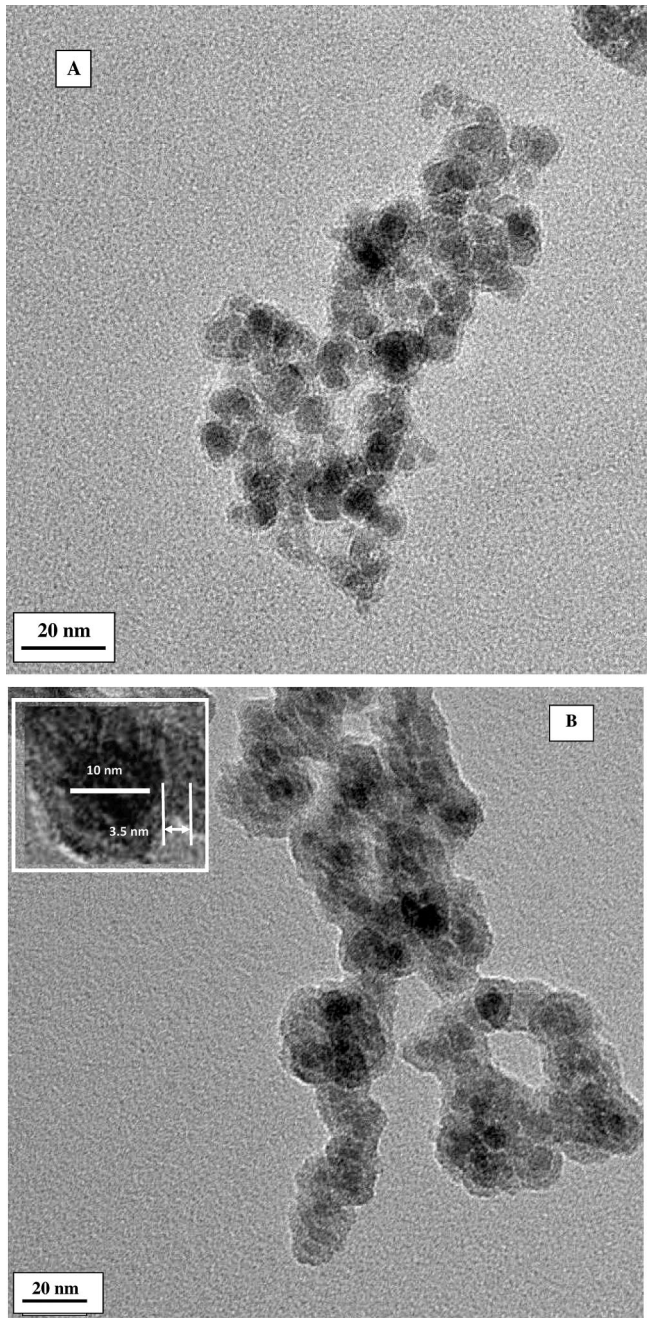

Figure 5. TEM images of Fe_3O_4@SiO_2 NPs after 1 h (A) and 3 h (B) of sonication. The scale bar is 20 nm. Zoomed image of a single core−shell particle is shown in the inset of panel b.

and at 4.2 K (Figure 7) may be interpreted as a superposition of doublet (superparamagnetic phase) and broad sextet (magnetic phase) peaks similar to that observed in other studies.[40,41] These spectra were fitted in two stages: (i) decomposition into Lorentzian lines presuming doublet for the superparamagnetic phase and two sextets for the magnetic phase and (ii) fitting of obtained broad lines using the Hesse−Rubartsch approach.[42] The spectra of Fe_3O_4@SiO_2 NPs at room temperature were treated by the same procedure. Calculated hyperfine parameters of Fe_3O_4 and Fe_3O_4@SiO_2 NPs are listed in Table 3. Then these parameters were used to estimate the percentage of superparamagnetic and magnetic phase in the prepared materials (Table 4).

Undoubtedly, the superparamagnetic behavior is due to the particle size effect. The large majority of prepared Fe_3O_4 NPs have a diameter in the range of 4−10 nm (Figure 1) which is much less than the theoretical value for the monodomain size of magnetite (~25 nm).[41] It seems to be reasonable to assume that the significant presence of magnetic phase in Mössbauer spectra of bare Fe_3O_4 NPs is related to the dipole−dipole interactions of magnetic nanoparticles according to eq 1. The sextet of magnetic phase which dominates at 4.2 K due to the blocking of Fe(III)−Fe(II) electron exchange does not exhibit a clear separation into tetrahedral (Td) and octahedral (Oh) sites typical for pure magnetite.[43] This effect has been recently interpreted as a formation of nonstoichiometric mixed oxide $(Fe^{3+})_{Td}[(Fe^{2+})_{1-3x}(Fe^{3+})_{1+2x}(\square)_x]_{Oh}O_4$, where □ is a vacancy formed due to the partial oxidation of Fe(II).[41,44] Although high-resolution XPS (Figure 3) clearly indicates the presence of Fe(II) at the surface of NPs some surface oxidation of magnetite cannot be completely excluded. Mössbauer spectrum will be, in this case, similar to that of nonoxidized Fe_3O_4 NPs, however, with a different area ratio for the subspectra. In practice, that leads to line broadening.

Figure 8 reveals that Mössbauer spectra of Fe_3O_4 NPs are strongly influenced by silica coating. Data in Table 4 clearly indicate that the coating of Fe_3O_4 NPs with silica causes the increase in the yield of superparamagnetic phase in an accordance with equations 1 and 2. It can be thus concluded that nonsuperparamagnetic behavior of Fe_3O_4@SiO_2 NPs observed with Mössbauer spectroscopy is mostly related to the dipole−dipole interactions of the magnetic cores and not to the particle size effect. This conclusion is of practical importance since it presumes principally superparamagnetic behavior of Fe_3O_4@SiO_2 NPs in colloids, where dipole−dipole attractions are much weaker than those in magnetic solids.

Magnetization **M** and coercivity $\mathbf{H_C}$ values obtained with SQUID technique at room temperature are summarized in Table 5. Corresponding magnetization curves for Fe_3O_4 and Fe_3O_4@SiO_2 NPs are shown in Supporting Information. It is seen that as the silica shell thickness increases, the observed **M** value is decreased, but its value per unit of magnetite is practically not influenced by coating. This confirms that sonochemical coating does not change the magnetic cores of NPs. The magnetization value of bare Fe_3O_4 NPs obtained in this work is close to that published in the literature[16] and is almost 2-fold less than the **M** value for micrometer-size range magnetite.[43] It is well-known that such decrease in magnetization is due to the effect of increased thermal fluctuation near the particle surface or to the magnetically disordered surface

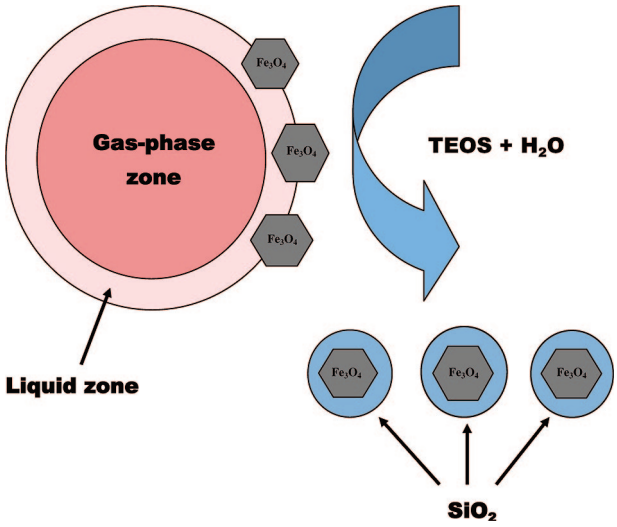

Figure 6. Schematic illustration of Fe_3O_4 NPs sonochemical coating with silica.

formed as a result of the large surface-to-volume ratio associated with the fine particle size.[33] Table 5 shows that Fe_3O_4@SiO_2 NPs obtained with sonochemistry exhibit a much higher magnetization value than that obtained under mechanical stirring. This could be assigned to better control of the silica quantities deposited under ultrasound as well as to the high speed of sonochemical coating, which prevents the magnetite from oxidizing.

All particles obtained in this work demonstrate a very low coercivity close to that of the theoretical value for superparamagnetic particles ($H_C \leq 5$ mT)[45] and much lower than that for the micrometer-size range magnetite. In contrast to Mössbauer spectra, the coercivity remains nearly constant upon silica coating. This phenomenon could be attributed to the high magnetocrystal-

TABLE 3. Hyperfine Parameters of Mössbauer Spectra for Fe_3O_4 and Fe_3O_4@SiO_2 NPs at Room Temperature

	δ (mm · s^{-1})	Γ (mm · s^{-1})	ε (mm · s^{-1})	Δ[a] (mm · s^{-1})	H^b (T)
Magnetic Td [Fe^{3+}]					
Fe_3O_4	0.29	0.35	0.001		7
Fe_3O_4@SiO_2, 1 h ultrasound	0.29	0.50	−0.06		34
Fe_3O_4@SiO_2, 3 h ultrasound	0.29	0.50	0.001	−23.4	
Magnetic Oh [Fe^{3+}, Fe^{2+}]					
Fe_3O_4	0.66	0.50	0.001		13
Fe_3O_4@SiO_2, 1 h ultrasound	0.66	0.50	0.001		36
Fe_3O_4@SiO_2, 3 h ultrasound	0.66	0.50	0.001		24.6
Superparamagnetic Td [Fe^{3+}]					
Fe_3O_4	0.29	0.30		0.85	
Fe_3O_4@SiO_2, 1 h ultrasound	0.29	0.40		1.43	
Fe_3O_4@SiO_2, 3 h ultrasound	0.29	0.30		0.93	
Superparamagnetic Oh [Fe^{3+}, Fe^{2+}]					
Fe_3O_4	0.66	0.30		0.90	
Fe_3O_4@SiO_2, 1 h ultrasound	0.66	0.40		1.97	
Fe_3O_4@SiO_2, 3 h ultrasound	0.66	0.30		1.19	

[a]Mean value of quadrupole splitting. [b]Mean value of hyperfine splitting.

TABLE 4. Magnetic and Superparamagnetic Phase Concentrations for Fe_3O_4 and Fe_3O_4@SiO_2 Nanopowders Calculated from Mössbauer Spectra

particles	magnetic (%)	superparamagnetic (%)
Fe_3O_4	61	39
Fe_3O_4@SiO_2 (1 h ultrasound)	48	52
Fe_3O_4@SiO_2 (3 h ultrasound)	37	63

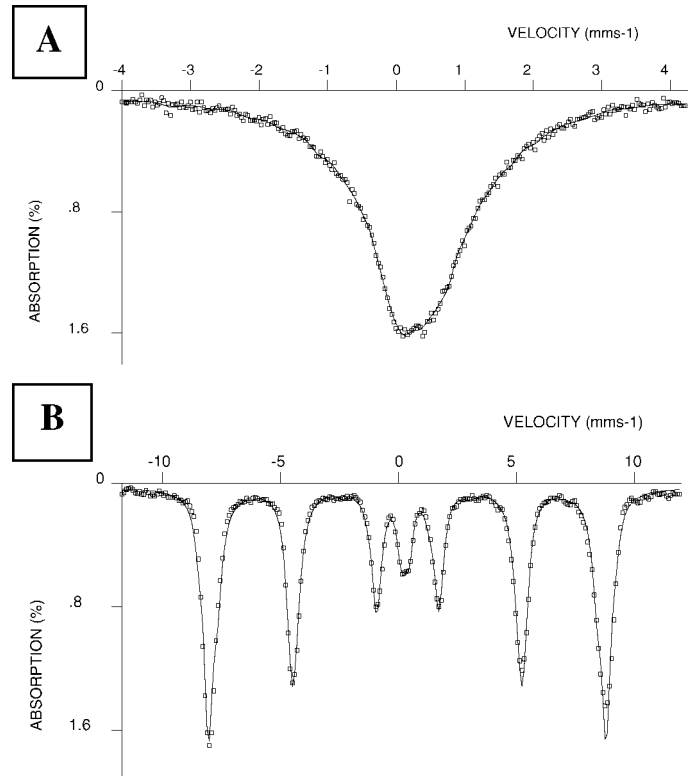

Figure 7. Mössbauer spectra of Fe_3O_4 NPs at room temperature (A) and at 4.2 K (B).

TABLE 5. Magnetic Properties of Fe_3O_4@SiO_2 NPs at Room Temperature

particles	M (emu · g^{-1})	M[a] (emu · g^{-1} Fe_3O_4)	H_c (mT)
Fe_3O_4 this work	51	51	8
Fe_3O_4,[16] (d∼15 nm)	55	55	
Fe_3O_4 bulk[43]	92	92	120−400
Fe_3O_4@SiO_2, 1 h of ultrasound	48	54	6
Fe_3O_4@SiO_2, 3 h of ultrasound	33	50	6
Fe_3O_4@SiO_2[16]	2−7		

[a]Calculated using FT-IR data and presuming insignificant influence of magnetite oxidation.

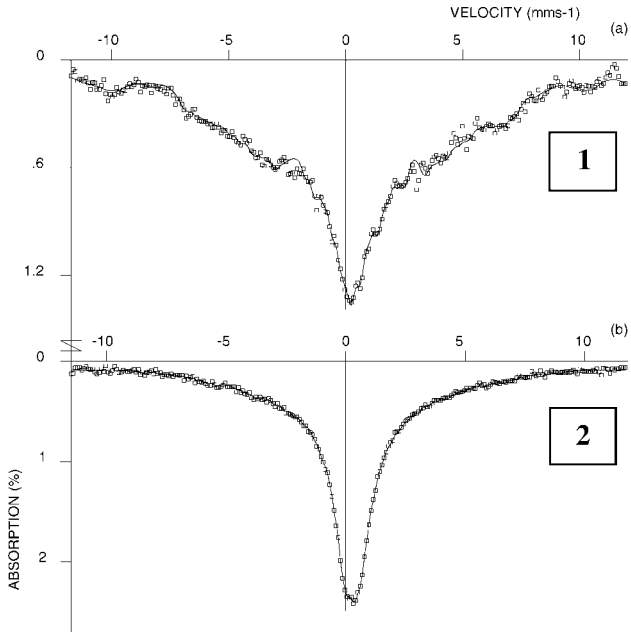

Figure 8. Mössbauer spectra of Fe_3O_4@SiO_2 NPs at room temperature obtained after 1 (A) and 3 h (B) of sonochemical coating.

line anisotropy of magnetite. The coercivity is defined as a measure of the magnetic field strength that is required to achieve changes of magnetization direction in a material. The observed $\mathbf{H_C}$ value is a combination of many anisotropy mechanisms, such as magnetocrystalline anisotropy, surface anisotropy, and interparticle interactions. It was reported that for small magnetite particles magnetocrystalline anisotropy is the dominant form of anisotropy.[43] Silica coating does not lead to any change in the shape and the size of magnetite cores and, therefore, would have little influence on the coercive force of the core−shell particles. A similar effect was observed recently for $CoFe_2O_4$@SiO_2 NPs also with high magnetocrystalline anisotropy.[46] Apparently, Mössbauer spectra exhibit higher sensitivity to the interparticle dipole−dipole magnetic interactions than SQUID measurements.

CONCLUSION

In this article, we reported a sonochemical approach to the synthesis of Fe_3O_4@SiO_2 core−shell NPs. First of all, it should be emphasized that coprecipitation of Fe(II) and Fe(III) in the ultrasonic field allows us to obtain smaller Fe_3O_4 NPs with narrow size distribution compared to those precipitated under mechanical stirring. Furthermore, we revealed that power ultrasound significantly accelerates alkaline TEOS hydrolysis in an alcohol−water mixture and in the presence of Fe_3O_4 NPs, hampers agglomeration, and improves the homogeneity of Fe_3O_4@SiO_2 NPs. It was shown that the thickness of the silica shell can be easily tailored with ultrasound in the range of several nanometers. Mössbauer spectroscopic study shows that silica coating improves the superparamagnetic behavior of magnetite nanopowder. From these measurements it follows that the presence of a magnetic component in Mössbauer spectra is attributed to dipole−dipole interactions between Fe_3O_4. Interestingly, the coercivity of magnetic NPs remains nearly constant upon silica coating which would be explained by the high magnetic magnetocrystalline anisotropy of magnetite.

EXPERIMENTAL SECTION

Sonochemical Setup. Ultrasonic treatment was performed in a thermostatically controlled tightly closed batch reactor with a volume of 50 mL. The sonoreactor was equipped with a titanium horn having 1 cm^2 of irradiating surface area and piezoelectric transducer supplied by a 20 kHz generator (Vibra Cell 600). The horn was immersed reproducibly below the surface of the sonicated liquid. The image of the experimental setup is available in Supporting Information. The temperature in the reactor during sonolysis was maintained using a Huber Unistat Tango thermocryostat. The experiments were performed at a steady-state temperature of 30−32 °C obtained after approximately 15 min of the sonication. Argon (<1 O_2 ppm) was bubbled at a rate of 100 $mL \cdot min^{-1}$ for about 30 min before sonication and during the ultrasonic treatment. The ultrasonic intensity, I ($W \cdot cm^{-2}$), and the specific absorbed acoustic power, P_{ac} ($W \cdot mL^{-1}$), transmitted to the solution were measured by the thermal probe method as described recently for the sonoreactors with similar geometry.[47] Typically the values of I and P_{ac} were equal to 30 $W \cdot cm^{-2}$ and 0.67 $W \cdot mL^{-1}$, respectively.

Preparation of Fe_3O_4 NPs. All aqueous solutions were prepared using deionized water (Milli-Q 18 MΩ). Ethanol, hydrochloric acid, and ammonia solutions were of highest purity. A freshly prepared mixture of 1.5 mmol $FeCl_3 \cdot 6H_2O$ (97%, Aldrich) and 0.75 mmol $FeCl_2 \cdot 4H_2O$ (99%, Aldrich) in 5 mL of 0.05 M HCl was rapidly injected *via* a fine plastic tube to 40 mL of 2 M ammonia solution containing 0.01 M of hydrazine (98%, Aldrich) under power ultrasound at 30−32 °C in an argon flow. Hydrazine reduced the redox potential of solution preventing Fe(II) from oxidizing. The injection was performed into the active zone of the sonoreactor *via* a fine plastic tube. Solids with a distinctive black color of magnetite were precipitated immediately after injection. The mixture was sonicated for 5 min. The sediment was transferred to a nitrogen filled glovebox, separated with a permanent magnet, and washed twice with argon purged 0.1 M NaCl solution and pure EtOH.

Preparation of Fe_3O_4@SiO_2 Core−Shell NPs. A suspension of 0.35 mmol freshly prepared Fe_3O_4 NPs in 30 mL of EtOH was sonicated for 15 min under argon, and then a chilled solution of 0.7 mL concentrated ammonia in 9.3 mL of water was added to the sonoreactor. This suspension was sonicated again for 15 min, and then a solution of 1.8 mmol TEOS (≥99%, Aldrich) in 5 mL of chilled EtOH was rapidly injected to the active zone of cavitation. The time of sonochemical treatment with TEOS was varied from 1 to 3 h at a steady-state temperature about 32 °C. A very stable black colored magnetic fluid was obtained even after 1 h of sonication. Silica-coated magnetite NPs were removed shortly after preparation by centrifugation at 15000 rpm for 30 min at a temperature of 10 °C. The precipitate was rapidly washed three times with chilled EtOH, and the final solids were redispersed in EtOH with power ultrasound (I = 30 $W \cdot cm^{-2}$, P_{ac} = 0.67 $W \cdot mL^{-1}$, τ = 15 min). Solid samples were obtained by EtOH evaporation at the reduced pressure in the entry-load chamber of an inert atmosphere glow box. A control experiment without ultrasound was performed under similar conditions with intensive mechanical nonmagnetic stirring in the presence of argon.

Characterization of Prepared Materials. Low-resolution TEM images were obtained with a Philips CM120 electron microscope

(120 keV) equipped with a USC1000 SSCCD 2k × 2k Gatan camera. A drop of tested colloid in EtOH was deposited on each carbon-coated copper grid (300 mesh) and dried in air.

The hydrodynamic diameter of Fe_3O_4@SiO_2 NPs in ethanol colloidal solutions was measured by using the quasi-elastic light scattering technique with a Malvern Zetasizer Nano ZS device.

Fourier transform infrared spectra (FT-IR) were recorded in KBr pellets with a Spectrum One Perkin-Elmer spectrometer. Calibration for the quantitative analysis of SiO_2 in the samples was performed at 1080 cm^{-1} (ν_{as} Si−O−Si) using pure SiO_2 in a KBr matrix. This calibration is shown in Supporting Information. One can see that absorbance at 1080 cm^{-1} is a linear function of SiO_2 content in the range of 0−0.6 mg of SiO_2 in the sample. Each value of absorbance was obtained as an average of three independent measurements.

XPS analysis was performed with an ESCALAB-220i-XL (THERMO-ELECTRON, VG Company) device. Photoemission was stimulated by a nonmonochromatized Mg Kα source (1253.6 eV) for uncoated Fe_3O_4 NPs and by a monochromatized Al Kα radiation (1486.6 eV) for more conductive Fe_3O_4@SiO_2 samples. An area of about 150 μm diameter was analyzed. The XPS spectra of Fe2p and Si2p were collected at a pass energy of 20 eV. Binding energies of these spectra were referenced to the C 1s binding energy set at 284.6 eV. The samples were pressed on to an indium support in a nitrogen-filled glovebox and then were put into the entry-load chamber to pump for approximately 12 h at room temperature under a pressure of about 10^{-7} Pa to minimize surface contamination. Small amounts of activated carbon fine powder were added to the samples to improve their conductivity.

The hysteresis cycle of powdered materials was measured using a QPMS SQUID magnetometer in the −4.5 to 4.5 T **H** range at room temperature. Particles were stabilized in epoxy resin matrix prior to measurements.

Mössbauer spectroscopy (MS) studies were carried out using a conventional constant acceleration HALDER-type spectrometer equipped with a ^{57}Co:Rh source. Metallic α-Fe was used as a reference. Powdered samples were placed in tightly closed cells within a nitrogen-filled glovebox. MS spectra were collected at room temperature and at $T = 4.2$ K with a helium cryostat. The MS spectra were refined in two steps. In the first treatment, Lorentzian peaks were assumed, and the position (isomer shift, δ), amplitude, and width of each peak were refined. This preliminary calculation allowed the determination of experimental hyperfine parameters for the various iron sites present in the samples. The second computation allowed the analysis of spectra in terms of hyperfine field distributions $P(\mathbf{H})$ and quadrupolar splitting distribution $P(\Delta)$ using the method of Hesse and Rubartsch.[42] This method is often used for disordered compounds with a strong line broadening and non-Lorentzian line profiles.

Acknowledgment. The authors gratefully acknowledge S.Vieules from MALVERN Instruments for her help in the DSL measurements.

Supporting Information Available: Details of the sonochemical device, the TEM images of Fe_3O_4 and Fe_3O_4@SiO_2 NPs, calibration curve for SiO_2 quantitative analysis with FT-IR, XPS spectra of Fe_3O_4 and Fe_3O_4@SiO_2 NPs, and magnetization curves for Fe_3O_4 and Fe_3O_4@SiO_2 NPs. This material is available free of charge *via* the Internet at http://pubs.acs.org.

REFERENCES AND NOTES

1. Olsvik, O.; Popovic, T.; Skjerve, E.; Cudjoe, K. S.; Hornes, E.; Ugelstad, J.; Uhlen, M. Magnetic Separation Techniques in Diagnostic Microbiology. *Clin. Microbiol. Rev.* **1994**, *7*, 43–54.
2. Widjojoatmodjo, M. N.; Fluit, A. C.; Torensma, R.; Verhoef, J. Comparison of Immunomagnetic Beads Coated with Protein A, Protein G, or Goat Anti-mouse Immunoglobulins. Applications in Enzyme Immunoassays and Immunomagnetic Separations. *J. Immunol. Methods* **1993**, *165*, 11–19.
3. Weissleder, R.; Elizondo, G.; Wittenberg, J.; Rabito, C. A.; Bengele, H. H.; Josephson, L. Ultrasmall Superparamagnetic Iron Oxide: Characterization of a New Class of Contrast Agents for MR Imaging. *Radiology* **1990**, *175*, 489–493.
4. Bulte, J. W. M.; Ma, L. D.; Magin, R. L.; Kamman, R. L.; Hulstaert, C. E.; Go, K. G.; The, T. H.; de Leij, L. Selective MR Imaging of Labeled Human Peripheral Blood Mononuclear Cells by Liposome Mediated Incorporation of Dextran-Magnetite Particles. *Magn. Reson. Med.* **1993**, *29*, 32–37.
5. Gupta, P. K.; Hung, C. T.; Lam, F. C.; Perrier, D. G. Albumin Microspheres. III. Synthesis and Characterization of Microspheres Containing Adriamycin and Magnetite. *Int. J. Pharm.* **1988**, *43*, 167–177.
6. Neuberger, T.; Schöpf, B.; Hofmann, H.; Hofmann, M.; von Rechenberg, B. Superparamagnetic Nanoparticles for Biomedical Applications: Possibilities and Limitations of a New Drug Delivery System. *J. Magn. Magn. Mater.* **2005**, *293*, 483–496.
7. Jordan, A.; Wust, P.; Fahling, H.; Scholz, R. Inductive Heating of Ferrimagnetic Particles and Magnetic Fluids: Physical Evaluation of Their Potential for Hyperthermia. *Int. J. Hyperthermia* **1993**, *9*, 51–58.
8. *Scientific and Clinical Applications of Magnetic Carriers*; Hafeli, U., Schutt, W., Teller, J., Zborowski, M., Eds.; Plenum Press: New York and London, 1997; pp 527−534..
9. Ito, A.; Hayashida, M.; Honda, H.; Hata, K.; Kagami, H.; Ueda, M.; Kobayashi, T. Construction and Harvest of Multilayered Keratonocyte Sheets Using Magnetite Nanoparticles and Magnetic Force. *Tissue Eng.* **2004**, *10*, 873–880.
10. Stöber, W.; Fink, A.; Bohn, E. Controlled Growth of Monodisperse Silica Spheres in the Micron Size Range. *J. Colloid Interface Sci.* **1968**, *1*, 62–69.
11. Bruce, I. J.; Taylor, J.; Todd, M.; Davies, M. J.; Borioni, E.; Sangregorio, C.; Sen, T. Synthesis, Characterization and Application of Silica-Magnetite Nanocomposites. *J. Magn. Magn. Mater.* **2004**, *284*, 145–160.
12. Yi, D. K.; Selvan, T.; Lee, S. S.; Papaefthymiou, G. C.; Kundaliya, D.; Ying, J. Y. Silica-Coated Nanocomposites of Magnetic Nanoparticles and Quantum Dots. *J. Am. Chem. Soc.* **2005**, *127*, 4990–4991.
13. Ma, Z.-Y.; Liu, X.-Q.; Guan, Y.-P.; Liu, H.-Z. Synthesis of Magnetic Silica Nanospheres with Metal Ligands and Application in Affinity Separation of Proteins. *Colloids and Surfaces A: Physicochem. Eng. Aspects* **2006**, *275*, 87–91.
14. Philipse, A. P.; van Bruggen, M. P. B.; Pathmamanoharan, C. Magnetic Silica Dispersions: Preparation and Stability of Surface-Modified Silica Particles with a Magnetic Core. *Langmuir* **1994**, *10*, 92–99.
15. Lu, Yu.; Yin, Y.; Mayers, B. T.; Xia, Y. Modifying the Surface Properties of Superparamagnetic Iron Oxide Nanoparticles Through a Sol-Gel Approach. *Nano Letters* **2002**, *2*, 183–186.
16. Deng, Y.-H.; Wang, C.-C.; Hu, J.-H.; Yang, W.-L.; Fu, S.-K. Investigation of Formation of Silica-Coated Magnetite Nanoparticles *via* Sol-Gel Approach. *Colloids and Surfaces A: Physicochem. Eng. Aspects* **2005**, *262*, 87–93.
17. Sun, Y.; Duan, L.; Guo, Z.; Duan Mu, Y.; Ma, M.; Xu, L.; Zhang, Y.; Gu, N. An Improved Way to Preparer Superparamagnetic Magnetite-Silica Core-Shell Nanopartilces for Possible Biological Application. *J. Magn. Magn. Mater.* **2005**, *285*, 65–70.
18. Santra, S.; Tapec, R.; Theodoropoulou, N.; Dobson, J.; Hebard, A.; Tan, W. Synthesis and Characterisation of Silica-Coated Iron Oxide Nanoparticles in Microemulsion: The Effect of Nonionic Surfactants. *Langmuir* **2001**, *17*, 2900–2906.
19. Momet, S.; Grasset, F.; Portier, J.; Duguet, E. Maghemite@silica Nanoparticles for Biological Applications. *Eur. Cells. Mater.* **2002**, *3*, 110–113.
20. Suslick, K. S.; Price, G. J. Applications of Ultrasound to Materials Chemistry. *Annu. Rev. Mater. Sci.* **1999**, *29*, 295–326.

21. Mason, T. J.; Lorimer, J. P. *Applied Sonochemistry. The Uses of Power Ultrasound in Chemistry and Processing.* Wiley-VCH Verlag GmbH: Weinheim, Germany, 2002; pp 53−55..
22. Suslick, K. S.; Choe, S.-B.; Cichowlas, A. A.; Grinstaff, M. W. Sonochemical Synthesis of Amorphous Iron. *Nature* **1991**, *353*, 414–416.
23. Gedanken, A. Using Sonochemistry for the Fabrication of Nanomaterials. *Ultrason. Sonochem.* **2004**, *11*, 47–55.
24. Abu Mukh-Qasem, R.; Gedanken, A. Sonochemical Synthesis of Stable Hydrosol of Fe_3O_4 Nanoparticles. *J. Colloid Interface Sci.* **2005**, *284*, 489–494.
25. Vijayakumar, R.; Koltypin, Yu.; Felner, I.; Gedanken, A. Sonochemical Synthesis and Characterization of Pure Nanometer-Sized Fe_3O_4 Particles. *Mat. Sci. Eng.* **2000**, *A286*, 101–105.
26. Dang, F.; Kamada, K.; Enomoto, N.; Hojo, J.; Enpuku, K. Sonochemical Synthesis of the Magnetite Nanoparticles in Aqueous Solution. *J. Ceram. Soc. Jpn.* **2007**, *115*, 867–872.
27. Rao, K.-S.; El-Hami, K.; Kodaki, T.; Matsushige, K.; Makino, K. A Novel Method for Synthesis of Silica Nanoparticles. *J. Colloid Interface Sci.* **2005**, *289*, 125–131.
28. Wang, J.; Loh, K. P.; Zhong, Y. L.; Lin, M.; Ding, J.; Foo, Y. L. Bifunctional FePt Core-Shell and Hollow Spheres: Sonochemical Preparation and Self-Assembly. *Chem. Mater.* **2007**, *19*, 2566–2572.
29. Ammar, M.; Mazaleyrat, F.; Bonnet, J. P.; Audebert, P.; Brosseau, A.; Wang, G.; Champion, Y. Synthesis and Characterization of Core-Shell Structure Silica-Coated $Fe_{29.5}Ni_{70.5}$ Nanoparticles. *Nanotechnology* **2007**, *18*, N285606.
30. Sun, C. Q. Size Dependence of Nanostructures: Impact of Bond Order Deficiency. *Progr. Solid State Chem.* **2007**, *35*, 1–159.
31. Scholten, P. C. In *Thermomechanics of Magnetic Fluids;* Berkovsky, B., Ed.; Hemisphere Publishing Corporation: Bristol, PA, 1978; pp 16−24.
32. Massart, R. Preparation of Aqueous Magnetic Liquids in Alkaline and Acidic Media. *IEEE Transactions on Magnetic* **1981**, *17*, 1247–1248.
33. Viota, J. L.; Duran, J. D. C.; Gonzalez-Caballero, F.; Delgado, A. V. Magnetic Properties of Extremely Bimodal Magnetic Suspensions. *J. Magn. Magn. Mater.* **2007**, *314*, 80–86.
34. Vayssières, L.; Chanéac, C.; Tronc, E.; Jovinet, J.-P. Size Tailoring of Magnetite Particles Formed by Aqueous Precipitation: An Example of Thermodynamic Stability of Nanometric Oxide Particles. *J. Colloid Interface Sci.* **1998**, *205*, 205–212.
35. Luque de Castro, M. D.; Priego-Capote, F. Ultrasound-Assisted Crystallization (Sonocrystallization). *Ultrason. Sonochem.* **2007**, *14*, 717–724.
36. Bund, R. K.; Pandit, A. B. Sonocrystallization: Effect on Lactose Recovery and Crystal Habit. *Ultrason. Sonochem.* **2007**, *14*, 143–152.
37. Descostes, M.; Mercier, F.; Thromat, N.; Beaucaire, C.; Gautier-Soyer, M. Use of XPS in the Determination of Chemical Environment and Oxidation State of Iron and Sulfur Samples: Constitution of a Data Basis in Binding Energies for Fe and S Reference Compounds and Applications to the Evidence of Surface Species of an Oxidized Pyrite in a Carbonate Medium. *Appl. Surf. Sci.* **2000**, *165*, 288–302.
38. Bruce, I. J.; Taylor, J.; Todd, M.; Davies, M. J.; Borioni, E.; Sangregorio, C.; Sen, T. Synthesis, Characterisation and Application of Silica-Magnetite Nanocomposites. *J. Magn. Magn. Mater.* **2004**, *284*, 145–160.
39. Suslick, K. S.; Hammerton, D. A.; Cline, R. E., Jr. The Sonochemical Hot Spot. *J. Am. Chem. Soc.* **1986**, *108*, 5641–5642.
40. Kim, D. K.; Mikhaylova, M.; Zhang, Yu.; Muhammed, M. Protective Coating of Superparamagnetic Iron Oxide Nanoparticles. *Chem. Mater.* **2003**, *15*, 1617–1627.
41. Kamali, M. S.; Ericsson, T.; Wäppling, R. Characterisation of Iron Oxide Nanoparticles by Mössbauer Spectroscopy. *Thin Solid Films* **2006**, *515*, 721–723.
42. Hesse, J.; Rubartsch, A. Model Independent Evaluation of Overlapped Mössbauer Spectra. *J. Phys. E* **1994**, *7*, 526–534.
43. Cullity, B. D. *Introduction to Magnetic Materials*, Addison-Wesley Publishing: Reading, MA, 1972, 410−421..
44. Nedkov, I.; Merodiiska, T.; Slavov, L.; Vandenberghe, R. E.; Kusano, Y.; Takada, J. Surface Oxidation, Size and Shape of Nano-Sized Magnetite Obtained by Co-Precipitation. *J. Magn. Magn. Mater.* **2006**, *300*, 358–367.
45. Heslop, D.; McIntosh, G.; Dekkers, M. J. Using Time- and Temperature-Dependent Preisach Models to Investigate the Limitations of Modeling Isothermal Remanent Magnetization Acquisition Curves with Cumulative log Gaussian Functions. *Geophys. J. Int.* **2004**, *157*, 55–63.
46. Vestal, C. R.; Zhang, Z. J. Synthesis and Magnetic Characterization of Mn and Co Spinel Ferrite-Silica Nanoparticles with Tunable Magnetic Core. *Nano Lett.* **2003**, *3*, 1739–1743.
47. Nikitenko, S. I.; Le Naour, C.; Moisy, Ph. Comparative Study of Sonochemical Reactors with Different Geometry Using Thermal and Chemical Probes. *Ultrason. Sonochem.* **2007**, *14*, 330–336.